Crystal structure of an aminoglycoside 6′-*N*-acetyltransferase: defining the GCN5-related *N*-acetyltransferase superfamily fold

Leanne E Wybenga-Groot, Kari-ann Draker, Gerard D Wright and Albert M Berghuis

Background: The predominant mechanism of antibiotic resistance employed by pathogenic bacteria against the clinically used aminoglycosides is chemical modification of the drug. The detoxification reactions are catalyzed by enzymes that promote either the phosphorylation, adenylation or acetylation of aminoglycosides. Structural studies of these aminoglycoside-modifying enzymes may assist in the development of therapeutic agents that could circumvent antibiotic resistance. In addition, such studies may shed light on the development of antibiotic resistance and the evolution of different enzyme classes.

Results: The crystal structure of the aminoglycoside-modifying enzyme aminoglycoside 6′-*N*-acetyltransferase type Ii (AAC(6′)-Ii) in complex with the cofactor acetyl coenzyme A has been determined at 2.7 Å resolution. The structure establishes that this acetyltransferase belongs to the GCN5-related *N*-acetyltransferase superfamily, which includes such enzymes as the histone acetyltransferases GCN5 and Hat1.

Conclusions: Comparison of the AAC(6′)-Ii structure with the crystal structures of two other members of this superfamily, *Serratia marcescens* aminoglycoside 3-*N*-acetyltransferase and yeast histone acetyltransferase Hat1, reveals that of the 84 residues that are structurally similar, only three are conserved and none can be implicated as catalytic residues. Despite the negligible sequence identity, functional studies show that AAC(6′)-Ii possesses protein acetylation activity. Thus, AAC(6′)-Ii is both a structural and functional homolog of the GCN5-related histone acetyltransferases.

Address: Department of Biochemistry, McMaster University, 1200 Main Street West, Hamilton, ON L8N 3Z5, Canada.

*Corresponding author.
E-mail: Berghuis@McMaster.Ca

Key words: antibiotic resistance, histone acetyltransferase, protein acetylation, structural similarity, X-ray crystallography

Received: 16 November 1998
Revisions requested: 12 January 1999
Revisions received: 11 February 1999
Accepted: 24 February 1999

Published: 28 April 1999

Structure May 1999, 7:497–507
http://biomednet.com/elecref/0969212600700497

Introduction

The increasing ability of bacteria to resist the effects of antibiotics, thus compromising the treatment of microbial infections, has provoked serious concern within the healthcare system [1–3]. The situation has, in fact, degenerated to such levels that bacterial strains have emerged that are immune to most, if not all, clinically useful antibacterial agents. Examples of these resistant microbes include vancomycin-resistant enterococci (VRE) and methicillin-resistant *Staphylococcus aureus* (MRSA), which have created havoc in hospitals [3–5]. The continuous evolution of antibiotic resistance by bacteria has motivated extensive research in this area, and much is currently known about the diverse mechanisms employed by bacteria for circumventing the deleterious effects of antimicrobial agents [6]. For example, the mechanism by which Gram-positive bacteria, like enterococci and staphylococci, circumvent the effects of aminoglycoside antibiotics, such as gentamicin and amikacin, is through chemical modification of the drug [7,8]. These clinically used drugs normally act by binding to the 16S ribosomal RNA [9,10], thus interfering with the translation of proteins and ultimately culminating in cell death. Chemical modification of the antibiotic, however, results in an altered affinity of the drug for its target, hence producing the antibiotic-resistant phenotype.

The chemical transformation of aminoglycoside antibiotics is catalyzed by a group of enzymes that are organized into three classes: those enzymes that *N*-acetylate, those that *O*-phosphorylate and those that *O*-adenylate the substrate [7,8]. This division into three classes does not imply that enzymes within a class are necessarily homologous at the amino acid level. For example, within the aminoglycoside acetyltransferase class (AAC) four different subclasses can be identified on the basis of the regiospecificity of acyl transfer, and within these subclasses several divisions exist based on amino acid sequence homology [7].

The three-dimensional structures of three aminoglycoside-modifying enzymes have been determined, one adenyltransferase (ANT(4′)-Ia) [11,12], one phosphotransferase (APH(3′)-IIIa) [13], and recently an acetyltransferase (AAC(3)-Ia) [14]. These structures have not only provided insight into the mechanism of antibiotic resistance at the atomic level, but, in addition, they have

established unexpected evolutionary links between bacterial aminoglycoside-modifying enzymes and several critical enzyme families present in eukaryotes. The crystal structure of the ANT(4′)-Ia enzyme shows homology to a eukaryotic DNA polymerase β, thus indicating that these enzymes may have evolved from a common ancestor [15]. The APH(3′)-IIIa structure reveals a striking, but unanticipated, similarity to protein kinases, thereby linking these two classes of enzymes [13]. Finally, the fold of AAC(3)-Ia is also observed in the yeast histone acetyltransferase Hat1 structure (yHat1) [16,17] and the *Candida albicans* and *Saccharomyces cerevisiae* *N*-myristoyltransferases (Nmt) [18–20].

The similarity in structure observed for AAC(3)-Ia and the yHat1 protein is of specific interest not only because it links these two enzymes, but in addition it provides insight into the fold of a large *N*-acetyltransferase superfamily, the GCN5-related *N*-acetyltransferase (GNAT) superfamily [21]. This superfamily spans all kingdoms of life and comprises more than a dozen protein families. These include, for example, the GCN5-related histone acetyltransferases, the yeast Mak3 and Spt10 proteins, and the pineal serotonin *N*-acetyltransferase.

We report here the structure of a second AAC enzyme, aminoglycoside 6′-*N*-acetyltransferase type Ii (AAC(6′)-Ii) in complex with acetyl coenzyme A (AcCoA). This 20.7 kDa antibiotic resistance protein was first identified in *Enterococcus faecium* by Courvalin and coworkers [22], and the gene for the protein was subsequently cloned and overexpressed in *Escherichia coli* [23]. This work opened the door for detailed studies on the mechanism of action of AAC(6′)-Ii, and to date the kinetic parameters for the acetylation of numerous aminoglycosides have been determined [23]. In addition, the conformation of two aminoglycosides when bound to the enzyme have been studied by NMR [24]. The structure of AAC(6′)-Ii establishes that this enzyme belongs to the GNAT superfamily; however, the overall appearance of the structure differs significantly from that of AAC(3)-Ia or yHat1. Examination of these three members of the GNAT superfamily provides insight into the structural diversity present within this family. Furthermore, the structure of AAC(6′)-Ii will provide an important framework for the development of inhibitory compounds that could reverse antibiotic resistance.

Results and discussion

The full-length structure of AAC(6′)-Ii (residues 1–182) in complex with AcCoA was determined by multiwavelength anomalous diffraction (MAD) using a selenomethionine-substituted protein. Diffraction data from a single crystal were collected at the CHESS F2 beamline under cryogenic conditions to a resolution of 2.7 Å (see Materials and methods section). The experimental electron-density map obtained was of excellent quality and a model for the enzyme could be readily traced (Figure 1). The structure has currently been refined to a crystallographic R factor of 18.8% and an R free of 23.4% using data between 40 and 2.7 Å with $F_{obs} > 1\sigma F_{obs}$ (i.e. 99.7% of all available data) [25]. The model contains 181 of the possible 182 residues, one AcCoA molecule and 28 ordered solvent molecules; the last residue in the sequence is disordered and was not modeled. The structure of the AAC(6′)-Ii–AcCoA complex displays good stereochemistry as assessed by the program PROCHECK [26] (e.g. 99% of nonglycine residues are placed within the favorable regions of the Ramachandran plot).

Figure 1

Experimental electron-density map of the AAC(6′)-Ii–AcCoA complex. The electron-density map was calculated to 2.8 Å resolution using MAD phases, generated from four selenium sites that were modified by the program SOLOMON [34,35]. The map is contoured at 1σ [34,35]. Shown is the region about the β bulge in strand β4 involving Pro75, which is in the *cis* conformation.

Architecture of the AAC(6′)-Ii enzyme

The AAC(6′)-Ii protein is a single domain structure consisting of α helices and β strands (Figures 2a and b). The shape of the molecule can be likened to an embellished letter V, with the AcCoA-binding site positioned in-between the two arms. Residues 1–103 make up the N-terminal arm (the right arm in Figure 2a), and residues 104–182 form the C-terminal arm. The core of the N-terminal arm of the molecule consists of a four-stranded antiparallel β sheet formed by strands β1 to β4 in the order β1-β2-β3-β4. Around this sheet are positioned three helices, one on top (α1), one in front (β2) and one behind the antiparallel β sheet (α3). The C-terminal arm of the molecule is built around a three-stranded antiparallel

Figure 2

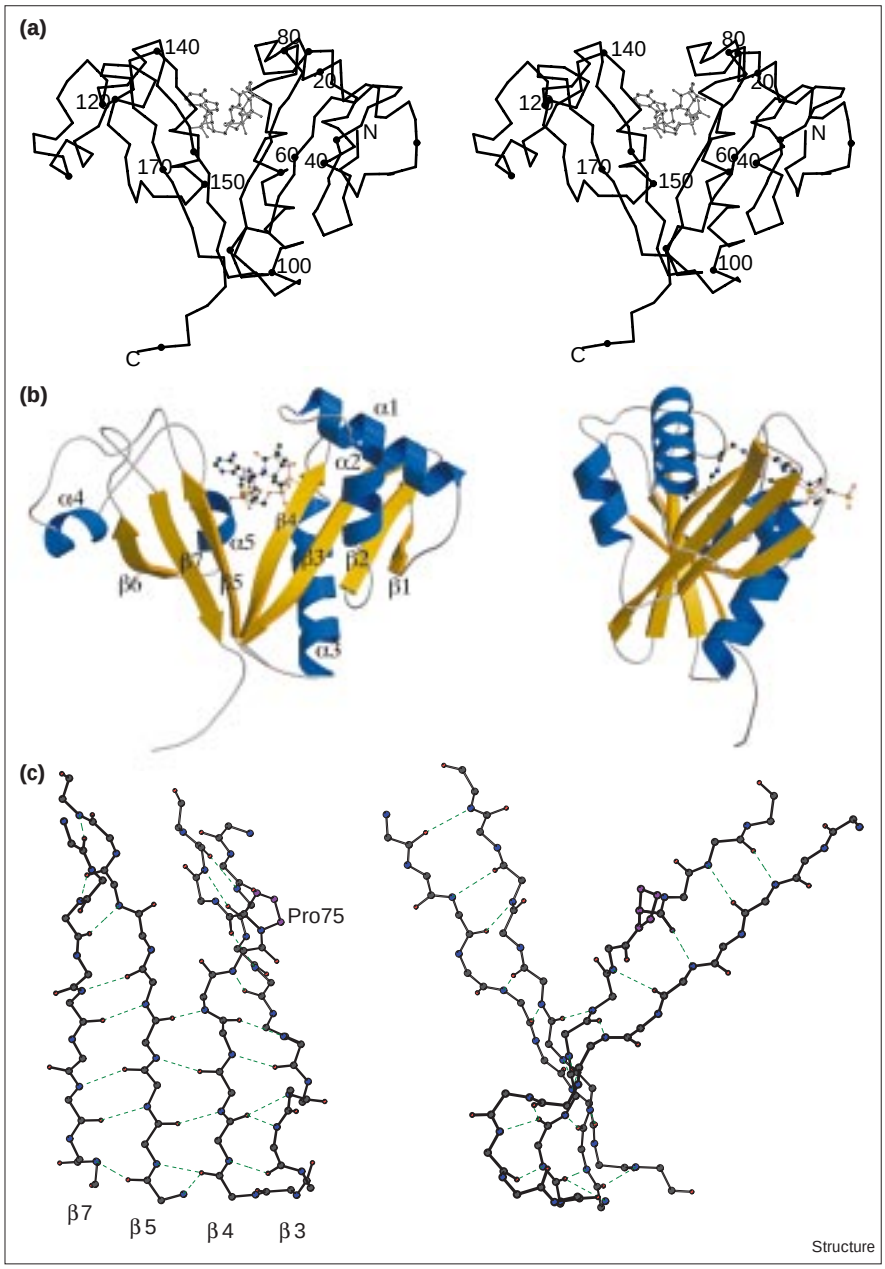

Schematic representations of the three-dimensional structure of the AAC(6′)-Ii–AcCoA complex highlighting different aspects of the fold. (a) Stereoview Cα trace of AAC(6′)-Ii–AcCoA in an orientation that emphasizes the likeness of the fold to an embellished letter V. (b) Drawing of the enzyme–AcCoA complex highlighting the different secondary structure elements: β strands are shown in yellow and α helices in blue. The bound AcCoA molecule is shown in ball-and-stick representation. The complex is shown in the same orientation as in (a) and also rotated 90° about the vertical axis. (c) A detailed view of the region where the N- and C-terminal arms are joined, focusing on the β bulge involving *cis* Pro75. Shown are the backbone atoms and hydrogen bonds for β strands β3–β7, plus all atoms of Pro75. The two orientations differ from each other by a 90° rotation about the vertical axis. (The figure was generated using BOBSCRIPT [40] and RASTER3D [41]; secondary structure elements were assigned using the program DSSP [42].)

β sheet, which has the order β5-β7-β6. This C-terminal β sheet is flanked by two helices, which are located on top (α4) and behind (α5) the sheet in the orientation shown in Figure 2a. The joint between the two arms is formed by the first five N-terminal residues of strand β4 and the first four residues of strand β5, which are parallel; thus, at the bottom of the letter V the N- and C-terminal sheets merge into a mixed parallel/antiparallel β sheet (Figure 2c). The C-terminal tail of the enzyme (residues 176–182), of which the last residue has poor to nonexistent electron density and was thus not included in the current model, is directed away from the molecule. This tail is for the most part in an extended conformation and forms no intramolecular interactions. However, examination of crystal packing reveals that the C-terminal residues that could reliably be modeled (residues 176–181) form extensive intermolecular interactions. Therefore, it is likely that in solution the seven C-terminal residues possess no rigid conformation, but are fully flexible.

The overall fold of the AAC(6′)-Ii molecule, as shown in Figures 2a and b, reveals an apparent pseudo-twofold

Figure 3

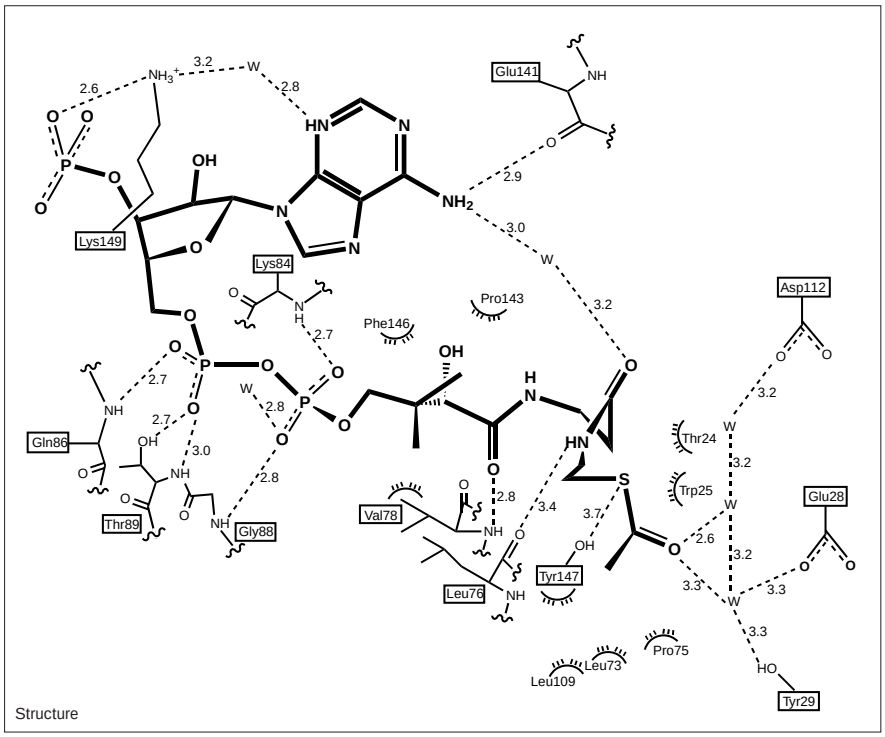

Interactions between the AcCoA cofactor and AAC(6′)-Ii. The AcCoA molecule and residues forming interactions with it are drawn schematically, with dashed lines indicating hydrogen-bond interactions and semicircles denoting hydrophobic contacts. Hydrogen-bond distances, as observed in the AAC(6′)-Ii–AcCoA crystal structure, are given in Ångstroms.

symmetry between the N- and C-terminal arms. In fact, the helix-helix-strand-strand motif in the N-terminal arm (α1-α2-β2-β3) can be overlaid convincingly with the identical motif in the C-terminal arm (α4-α5-β6-β7). This observation suggests that gene duplication might be one of the events in the evolution of this acetyltransferase enzyme. However, no sequence similarity, either at the amino acid level or the nucleotide level, can be discerned for the structurally homologous regions. Thus, it might be that the observed internal symmetry of AAC(6′)-Ii is purely coincidence. An alternative hypothesis is that the gene duplication event occurred too long ago to be apparent by sequence similarity, and can only be observed through structural similarity.

An intriguing structural feature of the AAC(6′)-Ii molecule is the region where the N- and C-terminal arms are joined. As described above, the first five residues of strand β4 (residues 69–73) and first four residues of β5 (residues 105–108) form a parallel β sheet, but after this point the two strands diverge (Figure 2c). The structural reason for this divergence is the presence of a β bulge in strand β4 [27]. Residues His74 and Pro75 of the β4 strand and Gly61 of the β3 strand form a classic narrow β bulge, resulting in a larger than usual twist in the N-terminal sheet. The β5 strand oriented parallel and adjacent to β4 is unable to accommodate this twist and therefore diverges. The kink created in strand β4 by the β bulge is further accentuated by the fact that Pro75 is in the infrequently observed *cis* conformation (Figures 1 and 2c).

Analytical gel-filtration experiments indicate that the AAC(6′)-Ii enzyme is a dimer in solution [23]. However, in the crystal form there is only one enzyme molecule in the asymmetric unit (see Materials and methods section). This observation most probably implies that the symmetry operator that relates the two molecules in the dimer species coincides with a crystallographic symmetry operator. Unfortunately, identifying the physiological dimer species in the crystal form is complicated by the high degree of symmetry present in the particular space group ($I4_132$), that is, there are six distinct dimers of which four are candidates for the physiological dimer, as judged by the extent of dimer interfaces. Thus, a definitive identification of the AAC(6′)-Ii dimer species will require the crystallization of AAC(6′)-Ii in another crystal form, and/or mutational studies of residues in putative dimer interfaces. Examination of the four candidates for the dimer species reveals that dimer formation is unlikely to be required for catalytic activity, however, as none of the possible dimer combinations possess a shared active site.

The AcCoA-binding pocket and substrate-binding site

The AcCoA molecule is wedged between the N- and C-terminal arms of the AAC(6′)-Ii molecule, forming interactions with both. Figure 3 depicts the various interactions

observed. Of the nine hydrogen bonds present between the enzyme and AcCoA, most are formed with the N-terminal arm of AAC(6′)-Ii (residues located on loop β4–α3 and helix α3), and only two are formed with the C-terminal arm (residues located on loop α4–α5 and helix α5). Furthermore, the majority of these hydrogen bonds are made with mainchain atoms, and only two sidechains interact with the AcCoA molecule: the Lys149 sidechain amino group forms a hydrogen bond/salt bridge with the 3′-phosphate of AcCoA and a water molecule mediated hydrogen bond with the adenine ring; and the Thr89 hydroxyl group interacts with the α-phosphate group. An additional sidechain–AcCoA interaction may exist between Tyr147 and the AcCoA sulfur atom (distance of 3.7 Å).

A noteworthy feature of the hydrogen-bond interactions observed between the cofactor and the enzyme is that the two peptide groups, which are incorporated into the pantothenic acid and β-mercaptoethylamine moieties, effectively extend the N-terminal β sheet by one additional strand. This pseudo-β-sheet extension emphasizes the importance of the β bulge in strand β4, for this structural feature allows strands β4 and β5 to separate sufficiently so as to make room for the additional pseudo-strand provided by the AcCoA molecule.

In addition to hydrogen-bond interactions, the AcCoA molecule makes extensive van der Waal's contacts with the enzyme. Specifically, the pantothenic acid and β-mercaptoethylamine moieties are surrounded by hydrophobic residues originating from both the N- and C-terminal arms (e.g. Thr24, Trp25, Leu76, Val78, Pro143 and Phe146). Furthermore, the binding pocket for the β-methyl group of the acyl moiety is lined with hydrophobic residues (Leu73, Pro75 and Leu109) and is deep enough to accommodate slightly larger groups, in agreement with the observation that propionyl-CoA is also a suitable cofactor for AAC(6′)-Ii [23].

Although the AAC(6′)-Ii crystal structure presented does not contain an aminoglycoside substrate molecule, the position of the AcCoA sulfur atom provides a clear indication where such a substrate must be bound for acetylation to occur in the ternary complex. Examination of the molecular surface of the AAC(6′)-Ii–AcCoA complex reveals that the sulfur atom of the cofactor is positioned at the bottom of a cleft created by the N- and C-terminal arms. Specifically, this cleft is formed by the sidechains of Trp25, Glu27, Glu28, Asp112 and Leu114 (Figure 4). The size of this cleft is not large enough to function as a binding site for the complete aminoglycoside substrate, and it is most likely that only the 6′-amino group will be positioned in this cleft so as to undergo acetylation. This observation is consistent with the broad specificity of the enzyme [23]. Where the remaining part of the aminoglycoside antibiotic will be bound, if it is bound in a specific manner as suggested by NMR studies [24], is less clear. Considering that aminoglycosides are invariably positively charged compounds, the obvious location is the front entrance to the cleft (Figure 4). The wall of this front entrance is lined by residues again originating from both the N- and C-terminal arms of the enzyme. The sidechains participating in this lining are predominantly negatively charged (i.e. Glu36, Glu39, Glu72 and Asp168), thus providing a complementary charged surface to the substrate. The presence of a negatively charged surface patch, presumably for promoting the binding of aminoglycosides, is also observed in all other aminoglycoside-modifying enzymes of known structure [8,14].

Figure 4

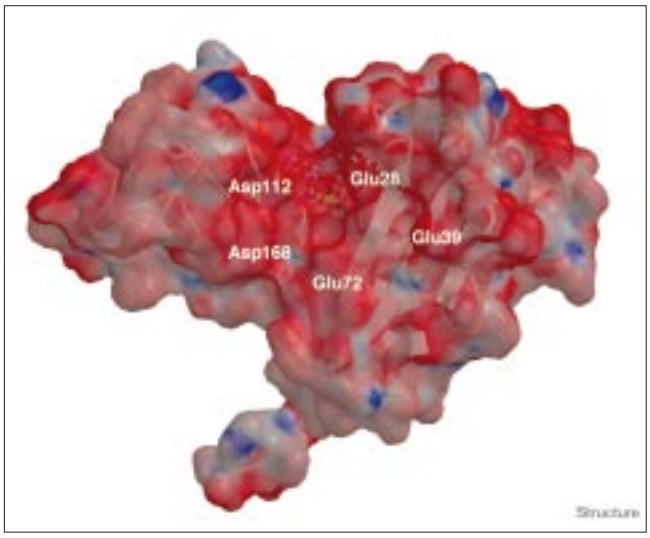

The putative aminoglycoside-binding site of AAC(6′)-Ii. The molecular surface of the AAC(6′)-Ii–AcCoA complex is colored according to electrostatic potential. The surface potential ranges from –10 to +10 k_BT (red to blue, respectively), as calculated using the program GRASP [43]. To highlight the position of the AcCoA sulfur atom, the molecular surface is partially transparent so that the AcCoA molecule and the AAC(6′)-Ii fold can be discerned. The orientation of the AAC(6′)-Ii–AcCoA complex is identical to that shown in the left panel of Figure 2b.

Comparison of AAC(6′)-Ii with other members of the GNAT superfamily

As mentioned above, part of the fold observed in AAC(6′)-Ii is seen in two other recently solved protein structures, yeast histone acetyltransferase Hat1 [16] and the aminoglycoside acetyltransferase from *Serratia marcescens*, also known as AAC(3)-Ia [14]. Thus, AAC(6′)-Ii belongs to the expansive GNAT superfamily of enzymes. The availability of crystal structures for three different members of the GNAT superfamily allows for a thorough analysis of the GNAT superfamily fold.

Figures 5a and b display the three-dimensional structures of AAC(3)-Ia, AAC(6′)-Ii and yHat1, and their secondary

Figure 5

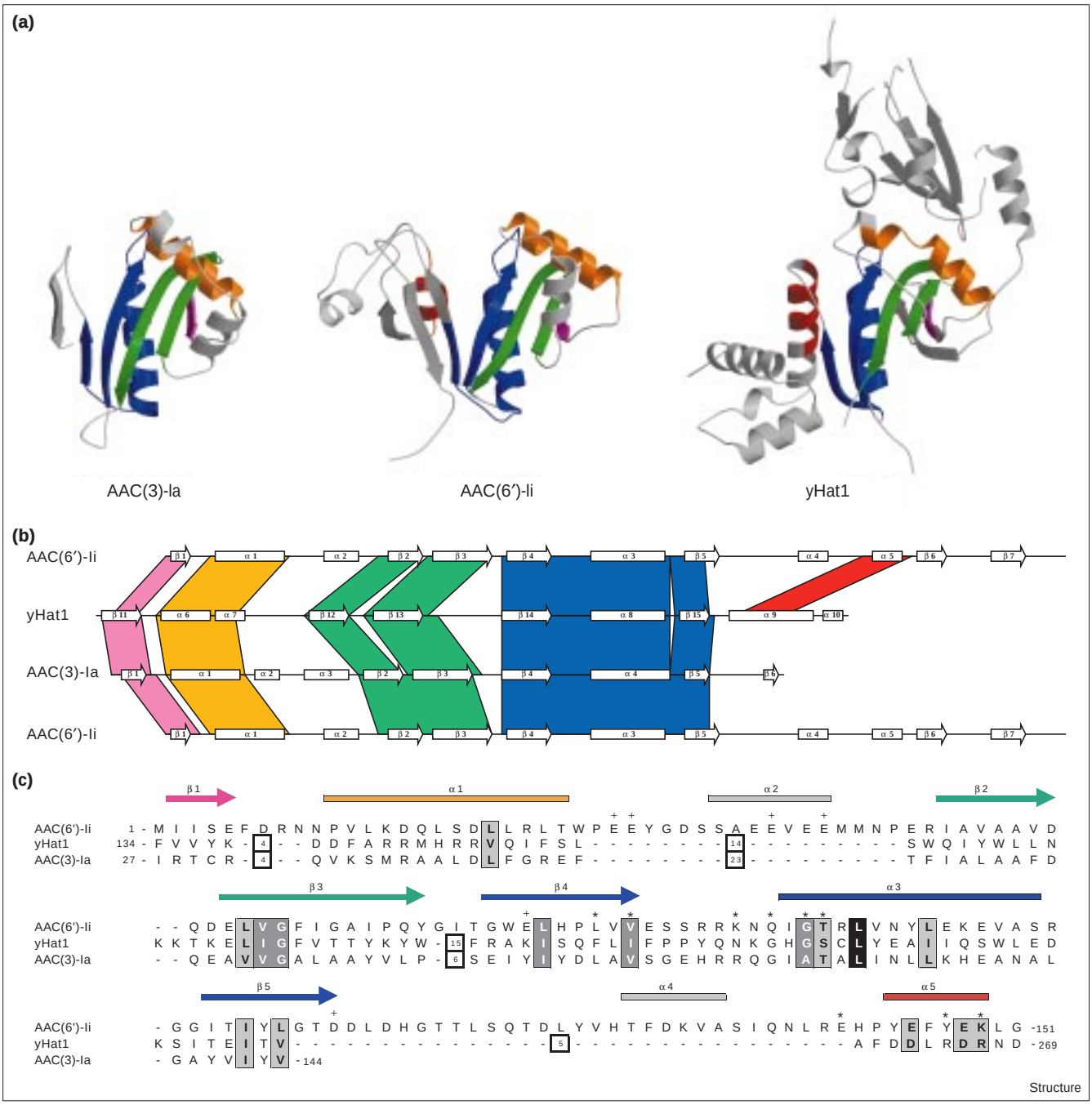

Structural comparison of AAC(6′)-Ii, yHat1 and AAC(3)-Ia. **(a)** Crystal structures of AAC(3)-Ia, AAC(6′)-Ii and yHat1 shown so as to highlight the common fold shared among GNAT superfamily members. To assist in the comparison, structurally similar regions are colored the same (i.e. purple, orange, green, blue and red), and dissimilar parts of the protein structures are colored white. **(b)** Linear representation of AAC(6′)-Ii, yHat1 and AAC(3)-Ia, highlighting the secondary structure elements and structurally similar regions. The color-coding used follows that described in (a). **(c)** Structure-based sequence alignment of the three GNAT superfamily members for which crystal structures have been determined. Residues that are functionally or absolutely conserved only within the AAC(6′)-Ii, AAC(3)-Ia and yHat1 structures are shown boxed with black lettering. Residues that are also functionally conserved within closely related sequences are shown boxed with a darkly shaded background and white lettering. Residues that are absolutely conserved within this larger sampling of GNAT superfamily members are shown boxed with a black background and white lettering. Inserts are shown as open boxes and the number displayed indicates the number of residues that are inserted at that location. The location of secondary structure elements is indicated and the color-coding scheme used follows that of (a) and (b). Residues that are known to interact with the cofactor are marked with an asterisk, and residues putatively implicated in substrate binding are indicated by a plus sign.

Table 1

Comparison between the AAC(6′)-Ii, yHat1 and AAC(3)-Ia crystal structures.

Compared structures	Number of residues*	Rms differences (Å)†
AAC(6′)-Ii and yHat1	94	2.44
AAC(6′)-Ii and AAC(3)-Ia	88	1.57
yHat1 and AAC(3)-Ia	89	2.41

*Number of residues that are in structurally similar locations (see Figure 5). †Root mean square (rms) difference in Cα positions between structurally similar residues.

structure elements. Virtually all of the AAC(3)-Ia structure, the N-terminal arm and part of the C-terminal arm of AAC(6′)-Ii, and the central core of yHat1 share a similar folding pattern (Table 1). Specifically, the N-terminal β sheet β1–β4 and helix α3 plus strand β5 (AAC(6′)-Ii nomenclature) are structurally well conserved. Interestingly, substantial variation can also be discerned. The notable differences between AAC(6′)-Ii and the other GNAT structures concern the presence or location of homologous helices α1, α2 and α5: helix α1 is partly unwound in the yHat1 acetyltransferase enzyme; helix α2 is shifted and preceded by an additional helix in AAC(3)-Ia and absent in yHat1; and helix α5 is completely absent in AAC(3)-Ia, while it is extended into a much longer helix in the yeast Hat1 structure (α9, yHat1 nomenclature).

The structural similarities and differences observed between the three available crystal structures of GNAT superfamily members is surprisingly not reflected in the sequence similarity. As shown in Figure 5c, of the 84 residues that are structurally identical in the three acetyltransferase structures, only three are chemically identical (3.6%) and nine are chemically similar (10.7%). Furthermore, if the sequence comparison is extended to include enzymes that are closely related (i.e. acetyltransferases that are more than 20% identical to AAC(6′)-Ii, yHat1 or AAC(3)-Ia, such as AAC(6′)-Ia, human Hat1 histone acetyltransferase and AAC(3)-Ig, respectively), the sequence similarity is even further reduced. Only one residue is consistently present (Leu91) and four are functionally conserved, Val/Ile57, Gly/Ala58, Leu/Ile73 and Gly/Ala88 (AAC(6′)-Ii numbering). Intriguingly, all of these residues are hydrophobic, suggesting that they are not required for catalysis, but instead are essential for cofactor binding and/or folding.

The virtual absence of conserved residues has implications for the manner in which the AcCoA cofactor is bound in GNAT superfamily members. Comparison of the interactions observed between the cofactor (either AcCoA or CoA) and AAC(6′)-Ii, yHat1 and AAC(3)-Ia, reveals that the predominant hydrogen-bond interactions are with mainchain amino and carbonyl groups. In fact, five of the

Figure 6

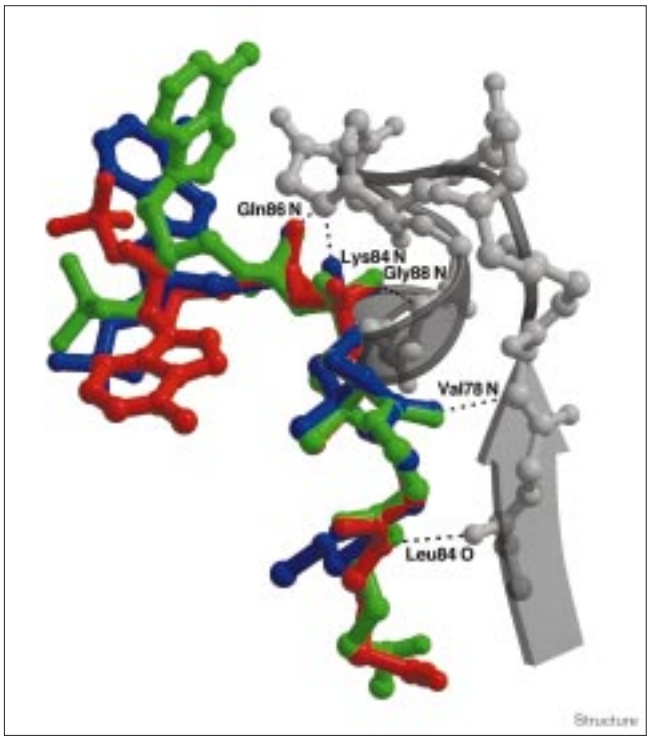

Cofactor conformations in AAC(6′)-Ii, yHat1 and AAC(3)-Ia. The figure shows the AcCoA conformations observed in AAC(6′)-Ii (red) and yHat1 (green), and the conformation of the CoA molecule seen in AAC(3)-Ia (blue). Also indicated are the five conserved hydrogen-bond interactions present between the cofactor molecules and the mainchain atoms of the different acetyltransferase enzymes. For clarity, only the mainchain atoms of AAC(6′)-Ii are shown (in gray), overlayed with the secondary structure assignment as a transparent object.

seven mainchain hydrogen bonds observed in AAC(6′)-Ii are conserved in both yHat1 and AAC(3)-Ia (Figures 3 and 6). The exceptions are the Glu141 hydrogen bond to the adenine ring, which is not observed in either yHat1 or AAC(3)-Ia, and the Thr89 amide interaction with the α-phosphate group, which is absent in the yHat1 crystal structure. On the other hand, the sidechain interactions present in the three GNAT superfamily structures are highly varied. This diversity is perhaps best illustrated by the observation that the adenine and ribose rings of the CoA moiety are in different conformations in the AAC(6′)-Ii, AAC(3)-Ia and yHat1 enzymes (Figure 6). One sidechain hydrogen bond consistently observed is the interaction between the hydroxyl group of residue Ser/Thr89 (124 in AAC(3)-Ia and 233 in Hat1) and the AcCoA α-phosphate group. This residue is not functionally conserved, however, (e.g. in AAC(6′)-Ia a lysine residue is located at this position).

Assessment of GNAT superfamily sequence motifs

As discussed above, a comparison of the three available crystal structures of GNAT superfamily members

reveals a near absence of absolutely conserved residues. Furthermore, examination of the AcCoA-binding site indicates that hydrogen-bond interactions with the cofactor are essentially sidechain independent. These observations suggest that sequence homology between GNAT superfamily members may be negligible. However, a novel multiple-alignment and database search procedure previously identified four conserved motifs, designated A to D, in the GNAT superfamily [21]. Of these motifs, all members possess motif A, and nearly all possess motifs B and D. Motif C is not always present, however; for example, the yHat1 enzyme and AAC(6′)-Ii do not have motif C. Given the structural similarity and diversity among the three GNAT superfamily members for which crystal structures are available, an evaluation of the structural basis for these sequence motifs is now possible.

Motif A physically starts at the N-terminal end of strand β4 and extends into helix α3 (AAC(6′)-Ii nomenclature). This motif contains three of the five (functionally) conserved residues identified — Leu/Ile73, Gly/Ala88 and Leu91 (AAC(6′)-Ii numbering) — which perhaps explains why sequence alignment methods were able to identify this motif. On the basis of mutagenesis studies, motif A has been implicated in the binding of the AcCoA cofactor (reviewed in [21]), which is consistent with crystal structure data. Many of the residues belonging to motif A either hydrogen bond to the cofactor or participate in hydrophobic interactions (Figure 3).

It has been proposed that motif B is also involved in cofactor binding [21]. However, validating this role proves problematic in that the physical location of this motif differs dramatically in the three available GNAT superfamily crystal structures. In AAC(6′)-Ii, motif B starts after helix α4 and includes helix α5 and strand β6. On the other hand, in the yHat1 crystal structure this same motif corresponds structurally to helices α9 and α10 (yHat1 nomenclature), of which helix α9 is partially homologous to the smaller helix α5 in AAC(6′)-Ii. Finally, motif B in AAC(3)-Ia starts after strand β5 and includes strand β6 (AAC(3)-Ia nomenclature). Note that strand β6 has no equivalence in either AAC(6′)-Ii or yHat1.

For the three acetyltransferase structures, motif C was thought to only be present in AAC(3)-Ia. In AAC(3)-Ia this motif corresponds to helix α1. As described above, the equivalent helix is also present in AAC(6′)-Ii (helix α1) and in yHat1, where it is partly unwound (helices α6 to α7). Therefore, the apparent absence of motif C based on amino acid sequence does not indicate the absence of the corresponding structural elements of this motif, but rather that the sequence homology at the amino acid level is undetectable.

Finally, motif D is present in all three acetyltransferase crystal structures. This motif starts halfway up strand β2 and terminates at the end of strand β3 (AAC(6′)-Ii nomenclature). The observation that not all GNAT superfamily members possess motif D is difficult to interpret as an absence of the corresponding structural feature (i.e. strands β2 to β3), considering the importance of the N-terminal β sheet for the fold of the enzyme. Rather, it may mean that the connecting loop between the two β strands has varying lengths, such that sequence similarity is difficult to detect.

Protein acetylation activity of AAC(6′)-Ii

Several lines of evidence indicated that AAC(6′)-Ii may have protein acetylation activity. Firstly, steady-state kinetics analysis yielded specificity constants (k_{cat}/K_m) in the order of 10^3–10^4 $M^{-1}s^{-1}$ for aminoglycoside substrates, well below the 10^6–10^8 $M^{-1}s^{-1}$ values usually associated with aminoglycoside-modifying and other antibiotic resistance enzymes [23]. Secondly, for aminoglycoside substrates, the steady-state parameter k_{cat} and not k_{cat}/K_m was positively correlated with the minimal inhibitory concentration of antibiotic, which is not consistent with an enzyme optimized for antibiotic detoxification [23]. Thirdly, the three-dimensional structure of AAC(6′)-Ii reveals a large cleft in the active-site region, which in principle can accommodate proteins (Figure 4). Finally, the structure shows similarity to yHat1, as described above (Figure 5; Table 1). We therefore investigated the protein acetylation capacity of purified AAC(6′)-Ii.

A survey of potential protein substrates, chosen on the basis of charge diversity and in-house availability, established that AAC(6′)-Ii can acetylate proteins. A mixture of calf histones enriched in H3 (15 kDa, pI = 11.5) and H4 (11 kDa, pI = 11.4), myelin basic protein (18 kDa, pI = 11.4), and ribonuclease A (16.5 kDa, pI = 8.6) were readily acetylated, and hen egg white lysozyme less so (16.2 kDa, pI = 9.1). In contrast, the aminoglycoside kinase APH(3′)-IIIa (30.9 kDa, pI = 4.4) and yeast homoserine dehydrogenase (38.5 kDa, pI = 7.35) were not substrates (data not shown). Thus, AAC(6′)-Ii is able to acetylate small basic proteins in a discriminate fashion. In addition to these potential protein substrates, spermidine and serotonin, which are positively charged substrates for two other members of the GNAT superfamily (i.e. spermidine *N*-acetyltransferase and serotonin *N*-acetyltransferase), were also tested (data not shown). Neither of these two compounds could be acetylated by AAC(6′)-Ii, demonstrating that the enzyme is selective in its activity, and does not merely acetylate any positively charged substrate.

We further investigated the acetylation of histones and poly-L-Lys (molecular mass ~1000 Da) to assess the nature of the acetyltransfer reaction. Histone acetylation

Figure 7

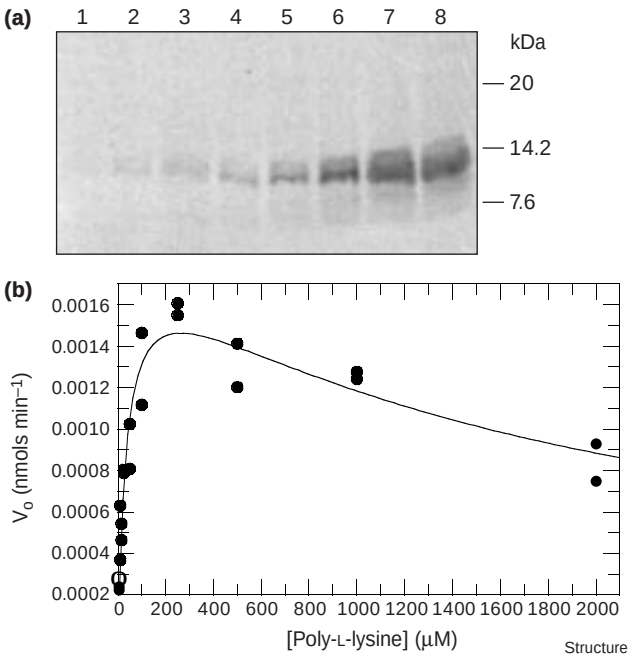

Protein acetylation by AAC(6′)-Ii. (a) The acetylation of histones. An autoradiogram of acetyltransferase reactions analyzed by sodium dodecylsulfate polyacrylamide gel electrophoresis shows the extent of histone acetylation catalyzed by AAC(6′)-Ii with increasing concentrations of protein substrate. Acetyltransferase reactions are as described in the Materials and methods section. The reactions were carried out with varying concentrations of histones: lane 1, 5 μM; lane 2, 10 μM; lane 3, 15 μM; lane 4, 25 μM; lane 5, 50 μM; lane 6, 100 μM; lane 7, 250 μM; lane 8, 500 μM. The positions of molecular mass standards are indicated. (b) Steady-state kinetics of acetylation of poly-L-Lys. Poly-L-Lys acetylation was monitored as described in the Materials and methods section. Data were fit to the equation $v = V_{max}S/(K_m + S + S^2/K_i)$, which describes substrate inhibition in the steady state.

was dependent upon substrate concentration (Figure 7a), consistent with enzymatic acyltransfer, but we did not achieve saturation due to the prohibitively high substrate concentrations required (> 1 mM). On the other hand, poly-L-Lys was a 'well behaved' substrate with a K_m of 38.5 ± 7.8 μM and k_{cat} of 0.0019 s^{-1} (Figure 7b). Like many aminoglycoside substrates, poly-L-Lys demonstrated substrate inhibition with a K_i of 1.78 mM, indicative of a non-productive binding mode. These results and the fact that 6′-hydroxyl-aminoglycosides are not substrates, but rather competitive inhibitors of AAC(6′)-Ii [23], support lysine *N*- rather than serine *O*-acetylation. These findings complement the observed structural homology between AAC(6′)-Ii and yHat1 with functional similarity, and strengthen the idea of an evolutionary relationship between the bacterial aminoglycoside acetyltransferases and the eukaryotic GCN5-related histone acetyltransferases.

Biological implications

Resistance to antibiotics by pathogenic bacteria, such as vanomycin-resistant enterococci (VRE) and methicillin-resistant *Staphylococcus aureus* (MRSA), severely complicates the treatment of microbial infections. One of the possible avenues to circumvent this complication is to inhibit the biochemical pathways that are responsible for generating the resistant phenotypes. The acetyltransferase AAC(6′)-Ii from the pathogen *Enterococcus faecium* is responsible for detoxifying a broad spectrum of aminoglycoside antibiotics, which are clinically used for the treatment of nosocomial infections. The crystal structure of this enzyme in complex with the cofactor acetyl coenzyme A (AcCoA) presents the necessary framework for pursuing the structure-based design of compounds that could obstruct the resistance mechanism for aminoglycoside antibiotics.

In addition to the practical implications of the AAC(6′)-Ii–AcCoA crystal structure for the treatment of bacterial infections, the fold of this enzyme reveals that AAC(6′)-Ii belongs to the GNAT superfamily. Structural studies of the GNAT superfamily have been nonexistent until very recently, even though this superfamily includes many critical enzymes, most notably the GCN5 histone acetyltransferase. To date, only three crystal structures of GNAT superfamily members have been determined, including the AAC(6′)-Ii structure presented here. Analysis of these three available structures reveals that the structurally conserved core, consisting of 84 residues, possesses minimal sequence homology. In fact, the few residues that are functionally conserved within this core are consistently hydrophobic, suggesting that they are not required for catalysis. This observation implies that the mechanism of acyltransfer for GNAT superfamily members is unlikely to incorporate a covalent acyl–enzyme intermediate.

Comparisons of the three acetyltransferase crystal structures revealed two structurally diverse regions — the C-terminal region after the fifth β strand and the polypeptide segment following the first helix — which straddle the AcCoA-binding site. It is probable that these two regions have a role in substrate specificity. Specifically, the segment in-between the first helix and strand β2 can function as a substrate specificity loop in GNAT superfamily members.

The structural similarity observed between the bacterial aminoglycoside acetyltransferase and the eukaryotic GCN5-related histone acetyltransferases posits an evolutionary linkage between these two classes of enzymes. This linkage is enforced by the observation that AAC(6′)-Ii is capable of acetylating small basic proteins in a discriminate manner, similar to histone acetyltransferases. However, the specific evolutionary pathway that

has resulted in the linkage between bacterial antibiotic resistance enzymes and eukaryotic enzymes involved in gene regulation is as yet unknown.

Materials and methods

Protein expression, purification and crystallization

The selenomethionyl derivative of AAC(6′)-Ii was obtained by transforming the *E. coli* methionine auxotroph B834(DE3)/pLys S with a pPLaac-1 overexpression plasmid containing the *aac(6′)-Ii* gene (GenBank accession code L12710) [23]. Cells were thereafter grown and the protein purified as described previously for the wild-type enzyme, with the exception that the growth medium used was that described by LeMaster and Richards supplemented with 50 mg/l of selenomethionine [23,28]. Mass spectrometry analysis of purified wild-type and selenomethionyl-derivatized enzymes revealed that all four methionine residues present were fully substituted by selenomethionine.

Conditions for crystallization were surveyed by the hanging-drop vapor diffusion technique using a commercially available sparse matrix screening kit (Hampton Research, Laguna Hills, CA) [29,30]. Promising conditions were subsequently refined, resulting in the following procedure. Reproducible, diffraction quality crystals were obtained by suspending a 6 µl drop, containing 7–10 mg ml^{-1} of protein, 2 mM AcCoA, 5% (w/v) D(+)-sucrose and 0.7 M ammonium sulfate, over a 1 ml reservoir of 2.0 M ammonium sulfate at 22°C. Cube-like crystals grew to average dimensions of $0.2 \times 0.2 \times 0.1$ mm in about two weeks. These crystals belong to the body-centered cubic spacegroup $I4_132$, with unit-cell dimensions of a = b = c = 147.0 Å, and one AAC(6′)-Ii molecule per asymmetric unit.

X-ray data collection, structure determination and refinement

Diffraction data were collected on the F2 beamline, equipped with a Quantum 4 ADSC CCD detector, at the Cornell High Energy Synchrotron Source in Ithaca, NY. Data at four different wavelengths, corresponding to the energy maxima for the real (λ_2) and imaginary (λ_3) components of the anomalous scattering, plus two wavelengths below (λ_1) and above (λ_4) the Se absorption edge, were measured at –170°C, from one crystal. Prior to data collection, this crystal had been briefly dipped in a 2.5 M ammonium sulfate solution saturated with D(+)-sucrose. Diffraction images thus obtained were processed to a resolution of 2.7 Å with the data reduction program MOSFLM [31] and programs from the CCP4 suite [32]. Positions for three of the possible four Se sites were subsequently determined with the SOLVE package [33] and refined using the program SHARP [34]. After density modification with SOLOMON [35], the coenzyme A moiety of the AcCoA molecule and 90% of the chain could be readily traced with the graphical program O [36]. This model was subjected to refinement using X-PLOR [37]. The improved phases thus generated allowed for the identification of the remaining Se site (Met1), and a new experimental map was calculated with SHARP/SOLOMON utilizing all four Se sites. This map was used throughout the refinement process to guide model building. Refinement of the model was hereafter continued, interspersed with manual interventions, which included completion of the protein structure and addition of ordered solvent molecules until no significant improvement could be obtained [38]. Pertinent statistics for data collection and phasing are shown in Table 2.

Acetyltransferase assays and steady-state kinetic analysis

Acetylation of histones, type VIII-S (Sigma) and poly-L-lysine (Sigma, MW ~1000 Da) by AAC(6′)-Ii was evaluated by a phosphocellulose-binding assay. Acetyltransferase reaction mixtures containing 25 mM HEPES pH 7.5, 1 mM EDTA, 0.1 µCi [1-^{14}C]AcCoA, 20 pmoles purified AAC(6′)-Ii, and varying concentrations of substrate, were incubated at 37°C for 10 min for poly-L-lysine and 15 min for histones. Reactions were applied to P81 cation exchanger chromatography paper (Whatman) and the samples washed at 70°C for 4 min followed by several 3 min rinses at 25°C to remove any reagents not bound to the phosphocellulose. Radioactivity incorporated into either poly-L-lysine or histones was counted using a Beckman LS 5801 series scintillation counter and the values baseline corrected. Steady-state kinetic parameters for poly-L-lysine were determined from initial velocities by direct fitting to an equation describing substrate inhibition using Grafit 3.0 software [39]. For visualization of histone acetylation by AAC(6')-Ii, acetyltransferase reaction mixtures were incubated at 37°C for 15 min and then separated on a sodium dodecyl sulfate (SDS) polyacrylamide gel followed by autoradiography.

Table 2

Summary of X-ray data and MAD phasing statistics.

	λ_1 (0.9809 Å)	λ_2 (0.9795 Å)	λ_3 (0.9792 Å)	λ_4 (0.9770 Å)
Data collection and processing statistics				
Resolution (Å)	2.8	2.7	2.7	2.7
Unique reflections	6085	7726	7725	7637
Redundancy	1.8	6.5	6.5	4.4
Completeness (%)*	89.7 (88.9)	99.9 (100.0)	99.8 (100.0)	99.1 (98.5)
R_{sym}*†	0.127 (0.332)	0.075 (0.188)	0.072 (0.170)	0.097 (0.263)
$\langle I/\sigma \rangle$*	4.3 (1.4)	8.8 (3.8)	9.3 (4.1)	4.9 (1.5)
Phasing statistics at 2.8 Å resolution				
Phasing power (four Se sites)‡				
isomorphous centric	0.45	0.32	–	0.71
isomorphous acentric	0.49	0.46	–	0.96
anomalous	–	1.37	2.19	1.09
Phasing power (three Se sites)‡				
isomorphous centric	0.41	0.26	–	0.65
isomorphous acentric	0.44	0.38	–	0.87
anomalous	–	1.31	1.95	1.06

*Numbers given in brackets refer to data for the highest resolution shell. †$R_{sym} = \Sigma|I-\langle I \rangle|/\Sigma\langle I \rangle$, where I is the observed intensity and $\langle I \rangle$ is the average intensity from multiple observations of symmetry-related reflections. ‡Statistics are provided for the phases derived from the complete heavy-atom model (four Se sites), and for the phases used to trace the initial model (three Se sites). All values were calculated with the SHARP package [34].

Accession numbers

The coordinates for the AAC(6′)-Ii–AcCoA complex have been deposited with the Protein Data Bank with accession code 1B87.

Acknowledgements

We thank the staff of MacCHESS for their technical support and advice during data collection at the Cornell University synchrotron facility in Ithaca, NY. We also thank Venkatraman Ramakrishnan of the University of Utah for providing us with coordinates of the yeast histone acetyltransferase Hat1–AcCoA complex and Stephen K Burley for providing us with coordinates of the AAC(3)-Ia–CoA complex, prior to release in the Protein Data Bank. Furthermore, our thanks goes to past and present members of the Wright and Berghuis laboratories for their assistance. This work was supported by grants from the Medical Research Council of Canada to AMB (MT-13107) and GDW (MT-13536). LEWG is the recipient of a Natural Sciences and Engineering Research Council of Canada graduate scholarship, and AMB is the recipient of a PMAC Health Research Foundation Research Career Award.

References

1. Cohen, M.L., Bloom, B.R., Murray, C.J.L., Neu, H.C., Krause, R.M. & Kuntz, I.D. (1992). Drug resistance. *Science* **257**, 1050-1082.
2. Travis, J., *et al.*, & Spratt, B.G. (1994). Frontiers in biotechnology: resistance to antibiotics. *Science* **264**, 360-393.
3. Williams, R.J. & Heymann, D.L. (1998). Containment of antibiotic resistance. *Science* **279**, 1153-1154.
4. Neu, H.C. (1992). The crisis in antibiotic resistance. *Science* **257**, 1064-1073.
5. Barie, P.S. (1998). Antibiotic-resistant gram-positive cocci: implications for surgical practice. *World J. Surg.* **22**, 118-126.
6. Davies, J. & Webb, V. (1998). Antibiotic resistance in bacteria. In *Emerging Infections.* (Krause, R.M., ed), pp. 239-273, Academic Press, San Diego, CA.
7. Shaw, K.J., Rather, P.N., Hare, R.S. & Miller, G.H. (1993). Molecular genetics of aminoglycoside resistance genes and familial relationships of the aminoglycoside-modifying enzymes. *Microbiol. Rev.* **57**, 138-163.
8. Wright, G.D., Berghuis, A.M. & Mobashery, S. (1999). Aminoglycoside antibiotics: structures, function and resistance. In *Resolving the antibiotic paradox: progress in drug design and resistance.* (Rosen, B.P. & Mobashery, S., eds), pp. 27-69, Plenum Publishing Corporation, New York, NY.
9. Fourmy, D., Recht, M.I., Blanchard, S.C. & Puglisi, J.D. (1996). Structure of the A site of *Escherichia coli* 16S ribosomal RNA complexed with an aminoglycoside antibiotic. *Science* **274**, 1376-1371.
10. Moazed, D. & Noller, H.F. (1987). Interaction of antibiotics with functional sites in 16S ribosomal RNA. *Nature* **327**, 389-394.
11. Sakon, J., Liao, H.H., Kanikula, A.M., Benning, M.M., Rayment, I. & Holden, H.M. (1993). Molecular structure of kanamycin nucleotidyltransferase determined to 3.0 Å resolution. *Biochemistry* **32**, 11977-11984.
12. Pedersen, L.C., Benning, M.M. & Holden, H.M. (1995). Structural investigation of the antibiotic and ATP-binding sites in kanamycin nucleotidyltransferase. *Biochemistry* **34**, 13305-13311.
13. Hon, W.C., *et al.*, & Berghuis, A.M. (1997). Structure of an enzyme required for aminoglycoside antibiotic resistance reveals homology to eukaryotic protein kinases. *Cell* **89**, 887-895.
14. Wolf, E., Vassilev, A., Makino, Y., Sali, A., Nakatani, Y. & Burley, S.K. (1998). Crystal structure of a GCN5-related N-acetyltransferase: *Serratia marcescens* aminoglycoside 3-N-acetyltransferase. *Cell* **94**, 439-449.
15. Holm, L. & Sander, C. (1995). DNA polymerase β belongs to an ancient nucleotidyltransferase superfamily. *Trends Biochem. Sci.* **20**, 345-347.
16. Dutnall, R.N., Tafrov, S.T., Sternglanz, R. & Ramakrishnan, V. (1998). Structure of the histone acetyltransferase Hat1: a paradigm for the GCN5-related N-acetyltransferase superfamily. *Cell* **94**, 427-438.
17. Travers, A. (1999). How to put a HAT on the histones. *Curr. Biol.* **9**, R23-R25.
18. Weston, S.A., *et al.*, & Pauptit, R.A. (1998). Crystal structure of the anti-fungal target N-myristoyl transferase. *Nat. Struct. Biol.* **5**, 213-221.
19. Bhatnagar, R.S., *et al.*, & Waksman, G. (1998). Structure of N-myristoyltransferase with bound myristoylCoA and peptide substrate analogs. *Nat. Struct. Biol.* **5**, 1091-1097.
20. Modis, Y. & Wierenga, R. (1998). Two crystal structures of N-acetyltransferases reveal a new fold for CoA-dependent enzymes. *Structure* **6**, 1345-1350.
21. Neuwald, A.F. & Landsman, D. (1997). GCN5-related histone N-acetyltransferases belong to a diverse superfamily that includes the yeast SPT10 protein. *Trends Biochem. Sci.* **22**, 154-155.
22. Costa, Y., Galimand, M., Leclercq, R., Duval, J. & Courvalin, P. (1993). Characterization of the chromosomal *aac(6′)-Ii* gene specific for *Enterococcus faecium*. *Antimicrob. Agents Chemother.* **37**, 1896-1903.
23. Wright, G.D. & Ladak, P. (1997). Overexpression and characterization of the chromosomal aminoglycoside 6′-N-acetyltransferase from *Enterococcus faecium*. *Antimicrob. Agents Chemother.* **41**, 956-960.
24. DiGiammarino, E.L., Draker, K.A., Wright, G.D. & Serpersu, E.H. (1998). Solution studies of isepamicin and conformational comparisons between isepamicin and butirosin A when bound to an aminoglycoside 6′-N-acetyltransferase determined by NMR spectroscopy. *Biochemistry* **37**, 3638-3644.
25. Brünger, A.T. (1992). Free R value: a novel statistical quantity for assessing the accuracy of crystal structures. *Nature* **355**, 472-475.
26. Laskowski, R.A., MacArthur, M.W., Moss, D.S. & Thornton, J.M. (1993). PROCHECK: a program to check the stereochemical quality of protein structures. *J. Appl. Crystallogr.* **26**, 283-291.
27. Richardson, J.S., Getzoff, E.D. & Richardson, D.C. (1978). The β bulge: a common small unit of nonrepetitive protein structure. *Proc. Natl Acad. Sci. USA* **75**, 2574-2578.
28. LeMaster, D.M. & Richards, F.M. (1985). ^{1}H-^{15}N heteronuclear NMR studies of *Escherichia coli* thioredoxin in samples isotopically labeled by residue type. *Biochemistry* **24**, 7263-7268.
29. Jancarik, J. & Kim, S.-H. (1991). Sparse matrix sampling: a screening method for crystallization of proteins. *J. Appl. Crystallogr.* **24**, 409-411.
30. McPherson, A. (1990). Current approaches to macromolecular crystallization. *Eur. J. Biochem.* **189**, 1-23.
31. Leslie, A.G.W. (1991) Macromolecular data processing. In *Crystallographic Computing.* (Moras, V.D., Podjarny, A.D. & Thierry, J.C., eds), pp. 27-38, Oxford University Press, Oxford, UK.
32. *Collaborative Computational Project Number 4.* (1994). The CCP4 suite: programs for protein crystallography. *Acta Crystallogr. D* **50**, 760-767.
33. Terwilliger, T.C. (1997). Multiwavelength anomalous diffraction phasing of macromolecular structures: analysis of MAD data as single isomorphous replacement with anomalous scattering data using the MADMRG program. *Methods Enzymol.* **276**, 530-537.
34. De La Fortelle, E. & Bricogne, G. (1997). Maximum-likelihood heavy-atom parameter refinement for multiple isomorphous replacement and multiwavelength anomalous diffraction methods. *Methods Enzymol.* **276**, 472-494.
35. Abrahams, J.P. & Leslie, A.G.W. (1996). Methods used in the structure determination of bovine mitochondrial F_1 ATPase. *Acta Crystallogr. D* **52**, 30-42.
36. Jones, T.A. & Kjeldgaard, M. (1993). O series, *Version 5.9*. Department of Molecular Biology, Uppsala University, Uppsala, Sweden.
37. Brünger, A.T. (1992). *X-PLOR: a System for X-ray Crystallography and NMR Version 3.1*. Yale University Press, New Haven, CT.
38. Kleywegt, G.J. & Brünger, A.T. (1996). Checking your imagination: applications of the free R value. *Structure* **4**, 897-904.
39. Leatherbarrow, R.J. (1992). *Grafit. Version 3.0.* Erithacus Software Ltd, Staines, UK.
40. Kraulis, P.J. (1991). MOLSCRIPT: a program to produce both detailed and schematic plots of protein structures. *J. Appl. Crystallogr.* **24**, 946-950.
41. Merritt, E.A. & Murphy, M.E.P. (1994). A program for photorealistic molecular graphics. *Acta Crystallogr. D* **50**, 869-873.
42. Kabsh, W. & Sander, C. (1983). Dictionary of protein secondary structure: pattern recognition of hydrogen-bonded and geometrical features. *Biopolymers* **22**, 2577-2637.
43. Nicholls, A., Sharp, K.A. & Honig, B. (1991). Protein folding and association: insights from the interfacial and thermodynamic properties of hydrocarbons. *Proteins* **11**, 281-296.